Scaling properties of particle density fields formed in simulated turbulent flows

Robert C. Hogan*
Symtech Incorporated, Alexandria, Virginia 22314

Jeffrey N. Cuzzi
NASA, Ames Research Center, Moffett Field, California 94035-1000

Anthony R. Dobrovolskis
University of California at Santa Cruz, Santa Cruz, California 95064
(Received 21 October 1998)

Direct numerical simulations of particle concentrations in fully developed three-dimensional turbulence were carried out in order to study the nonuniform structure of the particle density field. Three steady-state turbulent fluid fields with Taylor microscale Reynolds numbers (Re_λ) of 40, 80, and 140 were generated by solving the Navier-Stokes equations with pseudospectral methods. Large-scale forcing was used to drive the turbulence and maintain temporal stationarity. The response of the particles to the fluid was parametrized by the particle Stokes number St, defined as the ratio of the particle's stopping time to the mean period of eddies on the Kolmogorov scale (η). In this paper, we consider only passive particles optimally coupled to these eddies ($\mathrm{St}\approx 1$) because of their tendency to concentrate more than particles with lesser or greater St values. The trajectories of up to 70×10^6 particles were tracked in the equilibrated turbulent flows until the particle concentration field reached a statistically stationary state. The nonuniform structure of the concentration fields was characterized by the multifractal singularity spectrum $f(\alpha)$, derived from measures obtained after binning particles into cells ranging from 2η to 15η in size. We observed strong systematic variations of $f(\alpha)$ across this scale range in all three simulations and conclude that the particle concentration field is not statistically self-similar across the scale range explored. However, spectra obtained at the 2η, 4η, and 8η scales of each flow case were found to be qualitatively similar. This result suggests that the local structure of the particle concentration field may be flow independent. The singularity spectra found for 2η-sized cells were used to predict concentration distributions in good agreement with those obtained directly from the particle data. This singularity spectrum has a shape similar to the analogous spectrum derived for the inertial-range energy dissipation fields of experimental turbulent flows at $\mathrm{Re}_\lambda = 110$ and 1100. Based on this agreement, and the expectation that both dissipation and particle concentration are controlled by the same cascade process, we hypothesize that singularity spectra similar to the ones found in this work provide a good characterization of the spatially averaged statistical properties of preferentially concentrated particles in higher Re_λ turbulent flows. [S1063-651X(99)00807-7]

PACS number(s): 47.27.Eq, 47.11.+j, 47.53.+n, 47.55.Kf

I. INTRODUCTION

Particle-laden turbulent flows have been investigated in recent years by direct numerical simulations (DNS). A special behavior known as preferential concentration has been described as the tendency of particles to concentrate most strongly when their gas drag stopping times (τ_p) are close to the turnover time of the smallest turbulent structures (eddies and vortex tubes) [1–3]. This effect has also been observed in the laboratory [4,5].

The concentration process has been parametrized by the Stokes number St, defined as the ratio of τ_p to some eddy turnover time. Squires and Eaton [1,2] used the turnover time τ_Λ of the largest eddies, on the outer or integral scale Λ, where the energy that drives the turbulence is introduced. Instead Wang and Maxey [6], Eaton and Fessler [3], and this paper use the turnover time τ_η of the smallest eddies, on the inner or Kolmogorov scale η, the lowest scale of the turbulent cascade, where energy is dissipated. Particles with $\mathrm{St}=1$ so defined preferentially concentrate at spatial scales comparable to η [7]. Although it is not clear how turbulent structures direct the flow of particles into highly concentrated regions, the process is very sensitive to small deviations of St from this optimum value [8].

In this paper we focus on $\mathrm{St}=1$ particles and attempt to characterize the nonuniform structure of their concentration fields in a way that allows statistical predictions to be made over a wide range of turbulent flow strengths. We hypothesize that the nonuniform particle field is akin to the turbulent energy dissipation field whose statistical properties have been well described by the so-called ''singularity spectrum'' $f(\alpha)$ [9,10]. This spectrum has been shown to be both scale invariant and flow independent in the inertial and dissipation range of scales. Its interpretation as a multifractal dimension follows from its role as an exponent relating the spatial distribution of energy dissipation to scales that span the inertial

*Author to whom correspondence should be addressed. Address correspondence to Mail Stop 245-3, NASA Ames Research Center, Moffett Field, CA 94035-1000. Electronic address: hogan@cosmic.arc.nasa.gov

range. We believe the particle density field may also benefit from a multifractal analysis and may be aptly described by a singularity spectrum.

In Sec. II we present the governing equations and boundary conditions for the turbulent fluid and the particle trajectories. The numerical methods used to solve these equations and to evolve both the gas and particles to a statistically stationary state are described. We also include a table of simulation parameters for the three Reynolds numbers we studied, and explain why particular values were chosen. A measure for the particle concentration field and its role in the multifractal method is described in Sec. III. The emphasis in this section is on the practical aspects of determining the singularity spectrum. Useful numerical reductions that were employed to optimize the necessary computations are derived in the Appendix. Our results and interpretations are the subject of Sec. IV wherein we demonstrate how the singularity spectrum depends on the spatial binning size of the concentration measure and the flow Reynolds number Re_λ. A summary including remarks on this work and motivations for future work follows in Sec. V.

II. NUMERICAL SIMULATIONS

A. Gas and particle equations and boundary conditions

The equations governing the velocity field of an incompressible fluid and particles that respond with inertia to the drag forces are

$$U_{i,i}=0, \tag{1}$$

$$\frac{\partial U_i}{\partial t}+U_jU_{i,j}=-\frac{P_{,i}}{\rho}+\nu U_{i,jj}, \tag{2}$$

$$\frac{\partial V_i}{\partial t}=\frac{1}{\tau_p}\{U_i[X_i(t),t]- \quad V_i(t)\}, \tag{3}$$

where U is the gas velocity, V is the particle velocity, P is the gas pressure, ρ is the gas mass density, ν is the kinematic viscosity, and τ_p is the particle gas drag stopping time. Equation (2) is a simplified form derived by Squires and Eaton [1] that neglects corrections to the Stokes drag terms by assuming the mass density of a single particle is much greater than ρ and the particle size is much smaller than η. The influence of particles on the turbulence by momentum exchange is not considered in this study. The gas equations are solved in an Eulerian frame of reference relative to the mean flow, while Eq. (3) is solved in a Lagrangian frame.

The DNS code utilized in our study uses a modified version of the pseudospectral algorithm developed by Rogallo and Moin [11,12], and later extended by Squires and Eaton [1] to include gas-coupled particles. The code simulates forced stationary isotropic turbulence in a three-dimensional (3D) computational box 2π radians on a side. The forcing is introduced at the wave number $k_{\mathrm{forcing}}=\sqrt{14}$ with the scheme described by Eswaran and Pope [13]. Fluid velocities are found on a set of nodes uniformly spaced throughout the box. Periodic boundary conditions are imposed on the gas velocities at the sides of the computational domain. So while particles are free to roam outside of the computational box, their modulo 2π positions are employed when the fluid forces imparted to them are calculated. A third-order Taylor series interpolation scheme is used to determine force vectors at the folded particle positions from their values at the eight nearest neighbor nodes.

The pseudospectral algorithm's high degree of parallelism and vectorizable structure were exploited to implement it efficiently in the multitasking environment of the NAS Cray C90 facility. The particle integrations were also completely vectorized and executed as concurrent tasks on all 16 processors.

B. Reaching equilibrium

Before a detailed analysis of the particle concentration field was made, both the gas and particle components were fully evolved to a point of statistical equilibrium. The initial gas state of our first case was specified following the scheme by Lee and Reynolds [14], and in subsequent cases the equilibrated gas fields from previous runs were used. The gas, without particles, was evolved until the Kolmogorov scale (η) reached a steady value given by $\eta k_{\max}=1.3$, where $k_{\max}$ is the maximum useful wave number as determined by Rogallo's dealiasing scheme. This was done for a constant gas viscosity and node spacing by slowly adjusting the forcing strength for approximately six periods of the integral scale eddies. The particles were introduced, after the gas equilibrated, with zero velocities relative to the computational box, and at random locations therein. During the evolving phase the particles were binned periodically into a uniform grid of cells, centered over the computational nodes, in order to compute the rms value of the cell concentrations. The particle concentration field was considered to be equilibrated when the rms reached a steady value. This typically took another six large eddy turnover times. Following the procedure described above, we generated three statistically stationary turbulent fields at Re_λ values 40, 80, and 140, and evolved corresponding particle concentration fields containing 1×10^6, 10×10^6, and 70×10^6 particles, respectively. For each case, ten temporal realizations of the concentration fields separated by roughly one-half of a large eddy period were produced and archived.

C. Simulation parameters

The simulation parameters were selected to ensure adequate particle statistics and spatial resolution of the smallest turbulent scales. As the Reynolds number increases, the Kolmogorov scale structures shrink according to the scaling law $\eta\approx7.6\Lambda\,\mathrm{Re}_\lambda^{-3/2}$. More computational nodes are required to maintain a fixed resolution of the η scale as the Reynolds number is increased. More particles are also needed to maintain a useful population of particles within the more numerous η-scale concentration zones. In all three cases, the number of particles used was the number necessary to give an overall box-averaged cell concentration (N_{ave}) equal to at least 2 for cells 2η on a side. With this value, the initially uniform density of particles produced maximum cell occupancies ranging between 200 and 800 particles. Our interest in preferentially concentrated particles compelled us to consider only τ_p values close to the period of η-sized eddies. This period, known as the dissipation time scale τ_η, was calculated with the formula $\tau_\eta=\sqrt{\nu/\epsilon}$, where ϵ is the

TABLE I. Simulation parameters.

Parameter	Case I	Case II	Case III
Nodes/side	64	128	288
Viscosity	0.1	0.025	0.00625
N_p	10^6	10^7	7×10^7
Re_λ	39	79	141
Turbulent energy	40	23	12
Dissipation	204	74	27
$\eta k_{\max}$	1.4	1.3	1.3
η (radians)	0.047	0.021	0.0098
λ (radians)	0.44	0.28	0.17
Λ (radians)	0.58	0.44	0.35
τ_p	0.021	0.017	0.015
τ_η	0.022	0.018	0.015
τ_λ	0.2	0.3	0.47

volume-averaged energy dissipation [15]. Simulations of particle concentrations over a range of τ_p values were done in order to estimate the value that maximized the rms particle number density for bin sizes equal to 2η. The τ_p values for the $\mathrm{Re}_\lambda=40$ and 80 cases were found to be quite close to the dissipation time. The $\mathrm{Re}_\lambda=140$ case, however, could not be spanned as thoroughly because the computer time available to us allowed only a few τ_p values to be explored. For this case we assigned τ_p a value equal to τ_η.

The input and time-averaged output parameter values for each case are tabulated in Table I. Lengths are expressed in radians and times in computational units.

III. MULTIFRACTAL ANALYSIS

Fractal models of intermittence in turbulence have been developed to describe the cascade of energy from the largest to smallest eddies [10,16,17]. Measures generated by such processes are typically highly nonuniform and intermittent, and possess rich scaling properties. The observed scaling of the velocity structure constants provided the first test of these models [16,18,17]. Uniform fractal models, which assumed that turbulent energy was evenly divided among eddies of decreasing size, failed to predict these scalings. The assumption of a nonuniform partitioning of energy into smaller eddies led to multifractal models which proved a better match to the data [16,18]. A key element in the multifractal model is the singularity spectrum $f(\alpha)$. It serves as an exponent in the scaling laws for the velocity structure constants and other statistical measures.

The methods developed in recent years to analyze a variety of multifractal measures, including the energy dissipation field of fully developed turbulence, have inspired us to try them on the particle concentration fields generated in this study. This approach is well suited for describing the stationary statistical properties of processes far from equilibrium. In this section we describe how the method can be applied to the particle concentration field. We present mathematical expressions for quantities that characterize the field's nonuniform structure and can serve as exponents in scaling laws for concentration distribution functions.

A measure of the particle density field that is local, suitably normalized, and captures its nonuniformity is a key element in this analysis. The local measure we use is defined at a spatial scale l that is normalized relative to the computational box size. The measure is calculated by binning all N_p particles into a lattice of cubic cells, l on a side, that partition the computational volume uniformly into l^{-3} cells. Before they are assigned to a cell, particle positions are folded modulo 2π back inside the volume to ensure the inclusion of all simulation particles in the binning precedure. The average occupancy N_{ave} of a cell for a uniformly distributed particle field is $N_p l^3$. We define a cell's concentration factor by normalizing the number of particles found in the cell, N_i, by N_{ave},

$$C_i \equiv N_i / N_{\mathrm{ave}} = P_i l^{-3}, \tag{4}$$

where $P_i = N_i / N_p$ is interpretable as a probability measure and, as such, can be related to the cell size through the definition

$$P_i = l^{\alpha_i}. \tag{5}$$

For a given l, the set of exponents α_i provide an alternative description of the set of cell concentration factors.

In the limit $N_p \to \infty$, both P and α converge to a bounded continuum of values. Normalized volume and mass distribution functions for α can be written in forms that relate them, to first order, to the cell size,

$$F_V(\alpha)d\alpha = -\rho(\sqrt{\ln(1/l)}^{-f_l(\alpha)-3}d\alpha, \tag{6}$$

and

$$F_M(\alpha)d\alpha = -\rho\sqrt{\ln(1/l)}^{-f_l(\alpha)+\alpha}d\alpha, \tag{7}$$

where ρ is a constant of order unity and $f_l(\alpha)$ is the *singularity spectrum*. The l subscript serves as a reminder that the spectrum is in general a function of the cell size. The validity of these *Ansätze* has been demonstrated in an earlier study of the distribution of nearest neighbor distances of fractal sets [19].

In this paper we will be interested in the similarly normalized distribution functions for C which can be related to the above via the Jacobian transformation that relates C to α:

$$F_V(C)dC = F_V(\alpha)(dC/d\alpha)d\alpha \tag{8}$$

and

$$F_M(C)dC = F_M(\alpha)(dC/d\alpha)d\alpha. \tag{9}$$

The cumulative versions of these distributions are

$$F_V(>C) = \int_C^{C_{\max}} F_V(C)dC \tag{10}$$

and

$$F_M(>C) = \int_C^{C_{\max}} F_M(C)dC, \tag{11}$$

where $C_{\max}$ is C's upper bound.

The Appendix presents parametric expressions advocated by Chhabra and co-workers [20,9] to evaluate α and $f(\alpha)$ directly from the set of cell measures. These authors discuss

other direct methods for computing these scaling exponents and point out shortcomings that relate to their sensitivity to the logarithmic prefactors present in Eqs. (6) and (7). In the Appendix we derive alternative expressions that are more computationally efficient and make transparent their connection with the volume distribution of $P, F_V(P)$. These expressions are, from Eqs. (A5) and (A6),

$$\alpha_l(q) = \frac{\langle P^q \ln P \rangle}{\langle P^q \rangle \ln l}, \tag{12}$$

$$f_l(q) = \frac{\langle P^q \ln P^q \rangle - \langle P^q \rangle \ln \langle P^q \rangle}{\langle P^q \rangle \ln l} \tag{13}$$

where $\langle\ \rangle$ denotes an average over P weighted by $F_V(P)$.

The expressions above were used to evaluate α and f using discrete estimates of $F_V(P)$ derived from the particle concentration fields generated in our simulations.

IV. RESULTS

A. $\alpha(q)$, $f(q)$, and $f(\alpha)$

Both spatial and temporal realizations of the particle concentration field were generated and averaged in order to smooth out fluctuations. The spatial realizations were made by shifting the origin of the lattice of cells in each direction by half of a cell size. Ten temporal realizations were generated at intervals of approximately one-half the integral time scale τ_Λ.

For a single snapshot of the particle density field, the $F_V(P)$ distributions from all spatial realizations were averaged and the average was used to compute α and f using the formulas presented in the preceding section. They were evaluated on a 2D grid of l and q values. The l grid was uniformly spaced on a logarithmic scale in a range between 2η and 15η. The grid of q values was uniformly spaced between 0 and 20. Linear least squares fits to the set of exponents along the l direction were made for all values of q in order to interpolate between and extrapolate beyond the l grid points.

Figure 1 shows how α and f, determined from the $\mathrm{Re}_\lambda = 80$ simulations, vary with l at a selected set of q values. The abscissa is normalized relative to the η scale of the flow. In general, the exponents show a strong systematic dependency on cell size across the grid of scales. This scale dependence is made more evident in Fig. 2 where $(\alpha, f(\alpha))$ values are plotted for cell sizes equal to 2η, 4η, and 8η at all three Re_λ values.

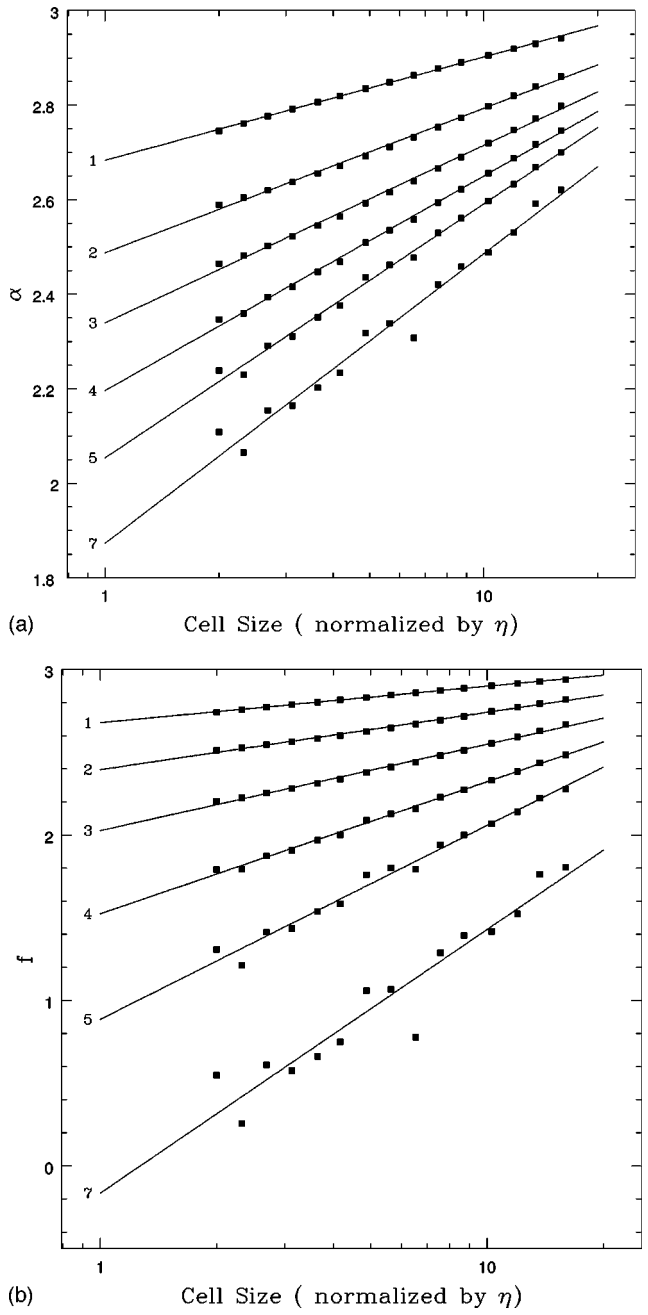

FIG. 1. (a) α and (b) f vs normalized cell size on a linear-log plot for a selected set of q values. Points represent averaged values calculated from ten temporal realizations of the particle concentration field formed in the $\mathrm{Re}_\lambda = 80$ flow simulations. Solid lines, labeled by q, represent linear least squares fits to the points and are extended to the η length scale. For all values of q both α and f vary strongly with cell size.

B. Correlation dimensions

From the singularity spectra we determined the correlation dimension, defined as $2\alpha - f$ at $q = 2$, for particle concentrations at the 2η scale. A value of 2.67 was found for all three simulations. A study of 2D projections of simulated particle concentrations in turbulent channel flows [21] reported a value of 1.68 for $\mathrm{St} = 1$ particles over a spatial scale where these particles are most concentrated. This compares well with our value after allowing for the difference between the support dimension of our measure (= 3) and theirs (= 2).

C. Concentration distributions

The singularity spectra shown in Fig. 2 were used to calculate $F_V(C)$ and $F_M(C)$ distributions, using Eqs. (6)–(9), for comparison with their discretized estimates. These predictions for the differential and cumulative distributions are presented in Figs. 3(a)–3(d). All discretized distributions included data from all temporal realizations of the particle density field. The cell size was 2η. The overall agreement suggests that the *Ansätze* used to represent the distributions

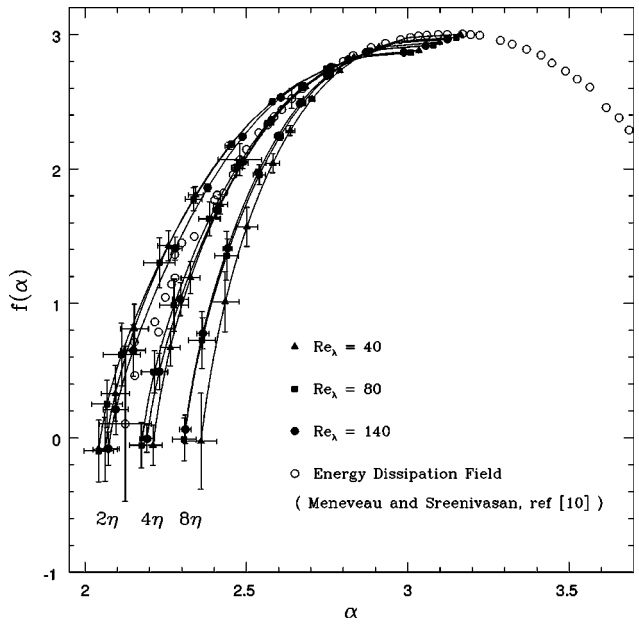

FIG. 2. Plots of $f(\alpha)$ vs α at cell sizes corresponding to 2η, 4η, and 8η. The f and α values were taken from line fits similar to the ones shown in Figs. 1(a) and 1(b). Symbols starting from the right correspond to q values 0,1,2,3,4,5,7,10,20. The error bars are the rms values derived from ten temporal realizations. The $f(\alpha)$ curves for cases $\mathrm{Re}_\lambda = 40$ (triangles), $\mathrm{Re}_\lambda = 80$ (squares), and $\mathrm{Re}_\lambda = 140$ (circles) have a similiar shape at all three length scales. Open circles are a composite of $f(\alpha)$ points presented in Fig. 10 of Meneveau and Sreenivasan [10] for turbulent energy dissipation derived from laboratory ($\mathrm{Re}_\lambda = 100$) and atmospheric ($\mathrm{Re}_\lambda = 1100$) data.

analytically are valid. The divergence at small C is probably due to the undersampling effects discussed in the Appendix.

D. The energy dissipation field

Velocity derivatives and passive turbulence scalars have previously been shown to have a multifractal character [18,22]. Specifically, the multifractal character of energy dissipation in turbulence is believed to be the result of a cascading process where energy at the largest scale trickles down to smaller scales in a nonuniform manner [16]. The singularity spectrum for energy dissipation has been derived from laboratory, atmospheric, and numerical data [9,23]. The spectrum shown by open circles in Fig. 2, taken from Fig. 10 in Meneveau and Sreenivasan [10], is a composite of results from flows at $\mathrm{Re}_\lambda = 100$ and 1100.

The shape and extent of the dissipation spectrum are very similiar to the singularity spectra for particle concentration, especially at the low-α end where dissipation and concentration are both greatest. The divergence between the concentration spectra towards $\alpha = 3$ reflects the incompleteness of the particle concentration measure, due to an insufficient number of particles to fill all the cells (see Appendix). We point out that the qualitative agreement in Fig. 2 may suggest a deep connection between the cascade process, presumed to control the flow of turbulent energy to smaller scales, and the process of particle concentration. This notion is consistent with the fact that strain rate is an important shared property of both particle accumulation [24,2] and dissipation.

V. SUMMARY AND DISCUSSION

In this paper we have investigated the stationary statistical properties of simulated number density fields of particles preferentially concentrated in turbulent flows. Singularity spectra, characterizing the nonuniformity of these fields, were derived to be used as exponents in analytical expressions for the $F_V(C)$ and $F_M(C)$ distributions. We found that the functional form of these spectra is sensitive to the binning scale of the concentration measure in all three flows. The spectra were found to be relatively insensitive to the turbulent flow strength when evaluated at cell sizes equal to 2η, 4η, and 8η. The analytical expressions are good predictors of the distribution functions when the derived $f(\alpha)$ spectra are used as the exponents. This result implies that the expressions used for the $F_V(C)$ and $F_M(C)$ functions, particularly the logarithmic, α-independent form of the prefactors, are correct and may be useful at higher Reynolds numbers.

St values other than 1

We have focused only on particles that have the strongest tendency to be concentrated, where the St of the particles is close to unity. It is likely that the scaling behavior we have discovered would also be found in particle fields characterized by St values other than unity. However, the singularity spectra would be expected to have a different relationship between f and α from the ones found in this study. For example, particles with substantially larger or smaller St concentrate much less, therefore making the minimum value of α larger and the spectrum steeper.

A homogeneous mix of particles with a wide range of St values could also be characterized by a singularity spectrum. This type of particle field might be more intimately connected with the turbulent energy dissipation process since it would be responsive to eddies across the hierarchy of size scales. Thus, we hypothesize that a multifractal analysis of such a mix would reveal singularity spectra more closely resembling the spectra derived from the energy dissipation measures of turbulence.

ACKNOWLEDGMENTS

We thank the Planetary Geology and Geophysics Program, and the Origins of Solar Systems Programs of NASA for support, and the NAS facility at Ames Research Center for computational resources. We also thank John Eaton and Kyle Squires for helpful conversations, and Alan Wray and Mike Rogers for their critical reviews of the manuscript.

APPENDIX

The expressions for $f(q)$ and $\alpha(q)$ described by Chhabra *et al.* [9] can be written as follows:

$$S(q) = \sum_{i=1}^{N_c} P_i^q, \tag{A1}$$

$$\alpha_l(q) \ln l = \frac{\sum_{i=1}^{N_c} P_i^q \ln P_i}{S(q)}, \tag{A2}$$

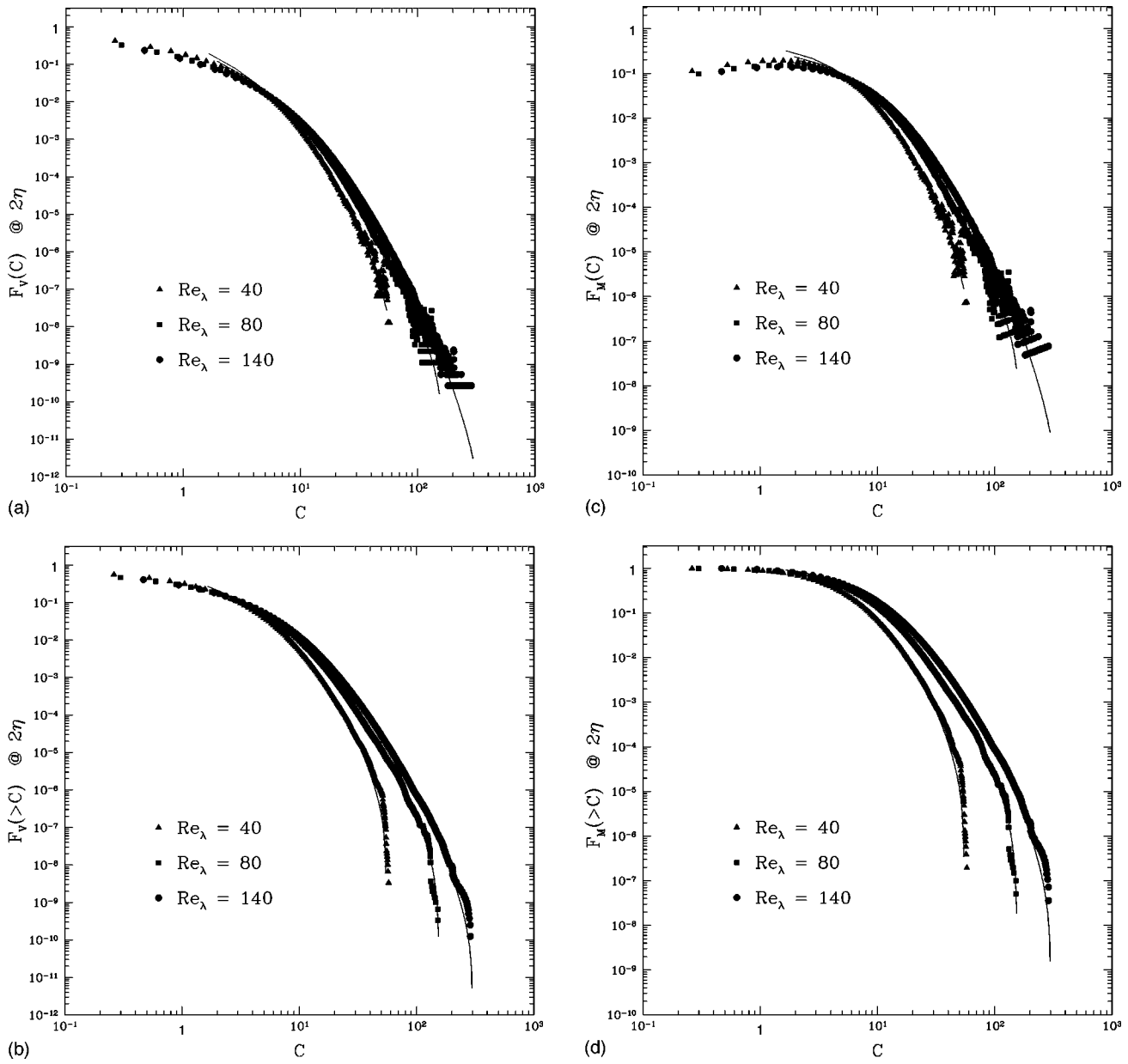

FIG. 3. (a) $F_V(C)$, (b) $F_V(>C)$, (c) $F_M(C)$, (d) $F_M(>C)$ concentration distributions derived directly from the binned particle data sets. The binning scale is 2η. Symbols label the three flow cases and the solid lines are the corresponding analytical predictions using the $f_{2\eta}(\alpha)$ derived from the $F_V(C)$ distributions. The overall agreement supports the validity of the functional form of the analytical expressions.

$$f_l(q)\ln l = \frac{\sum_{i=1}^{N_c} P_i^q \ln P_i^q - S(q)\ln S(q)}{S(q)}, \qquad \text{(A3)}$$

where P_i is a normalized measure of the occupancy of cell i, l is the cell size, N_c is the number of nonzero cell measures, and q is a real number between $+\infty$ and $-\infty$.

The derivation of these expressions is based on a formal relationship to thermodynamics that starts with an analogue of the partition function and leads to the Boltzmann averages that Eqs. (A2) and (A3) represent. These averages are considered more informative about the values of $f(\alpha)$ and α in cases when l cannot be taken to zero. P_i represents a probability for measures that arise from multiplicative processes. We have assumed in this study that the particle concentrations are also a consequence of such processes. The measure we believe is appropriate for the particles and analogous to the dissipation measure used by Chhabra *et al.* [9] is $P_i \equiv N_i/N_p$.

The limits $l\to 0$ and $N_p\to\infty$

Usually the expressions (A2) and (A3) are defined in the limit $l\to 0$ or $N_c\to\infty$. For a particle concentration field this limiting procedure would also require the measure P to reach convergence as $N_p\to\infty$. We have taken a more practical approach by focusing on how $f(\alpha)$ depends on l. The lower cutoff on the size of turbulent eddies would prevent scale-invariant behavior in the inertial range from continuing unabated into scales smaller than η. Thus, for our purposes, the limit $l\to\eta$ is physically meaningful. However, $N_p\to\infty$ needs

to be considered in order to verify our assumption that the singularity spectrum, or at least a useful portion of it, converges in this limit for values of l comparable to η. We have explored the convergence behavior of $f(\alpha)$ within the constraints that the available computer memory places on N_p. At the smallest l we used we found that a good portion of the spectrum converged when N_p was such that $N_{\rm ave}>2$. The part that converged corresponded to the denser regions of the particle field. The more rarified regions are represented as α increases towards 3. In this regime, both α and f become more sensitive to the number of unoccupied cells, which depends strongly on N_p. Unfortunately, we could not make N_p large enough to fill every cell for the smallest bin sizes used in our study. As a result, f and α diverge increasingly from their limiting values as $q\rightarrow 0$.

As is clear from Eqs. (A2) and (A3), summations over all N_c cells are required for each value of q. The construction of the cell measures involves summing over all N_p particles, and this must be repeated every time l is changed. Furthermore, both N_p and N_c need to be increased significantly between $\mathrm{Re}_\lambda = 40$ and 140 in order to maintain good particle statistics and resolve the η-scale particle density fluctuations. Because of the above considerations and the limited time and memory resources available to us on the Cray C90 we derived more efficient expressions to replace Eqs. (A1)–(A3).

The cell measures P_i are quantized by the amount $1/N_p$; that is, P can have only values $P_j = j/N_p$, $\quad j = 1, N_{\rm max}$. This implies that the summands in Eqs. (A1)–(A3) are also quantized. These summands can then be split into disjoint sets where the elements in a given set are all identical in value $(=P_j)$. Multiplying the number of elements of set j by P_j gives a quantity that represents the total contribution of set j to the overall sum. Summing over all sets in this way is an equivalent way of evaluating Eqs. (A2) and (A3). The size of these disjoint sets is, in our context, equivalent to the volume of space a set occupies. Thus, we can replace sums over cells with sums over disjoint sets weighted by the volume distribution function for P, $F_V(P_j)$, as $\Sigma_{i=1}^{N_b}(\cdots) \Rightarrow \Sigma_{j=1}^{N_{\rm max}}(\cdots)F_V(P_j)$, where $N_{\rm max}$ is the number of P_j bins.

The advantage of this replacement in our problem is that $N_{\rm max}$ is vastly smaller than N_c when $l \approx \eta$, and the histogram of $N_{\rm max}$ bins, once built, is used for all values of q. $N_{\rm max}$ depends on l, N_p, and the efficiency of the particle concentration process, but in practice is determined after all N_p particles in all realizations have been binned.

Equations (A1)–(A3) can then be rewritten as

$$S(q) \equiv \langle P^q \rangle, \tag{A4}$$

$$\alpha_l(q) \ln l \equiv \frac{\langle P^q \ln P \rangle}{\langle P^q \rangle}, \tag{A5}$$

$$f_l(q) \ln l \equiv \frac{\langle P^q \ln P^q \rangle - \langle P^q \rangle \ln \langle P^q \rangle}{\langle P^q \rangle}, \tag{A6}$$

where $\langle \cdots \rangle \equiv \Sigma_{j=1}^{N_{\rm max}} \cdots F_V(P_j)$ and $\Sigma_{j=1}^{N_{\rm max}} F_V(P_j) dP_j = 1$.

[1] K. D. Squires and J. K. Eaton, Stanford University Technical Report No. MD-55 (1990).
[2] K.D. Squires and J.K. Eaton, Phys. Fluids A **3**, 1159 (1990).
[3] J.K. Eaton and J.R. Fessler, Int. J. Multiphase Flow Suppl. **20**, 169 (1994).
[4] E.K. Longmire and E.K. Eaton, J. Fluid Mech. **236**, 217 (1992).
[5] L. Tang *et al.*, Phys. Fluids A **4**, 2244 (1992).
[6] L.P. Wang and M.R. Maxey, J. Fluid Mech. **256**, 27 (1993).
[7] A.R. Dobrovolskis *et al.*, Bull. Am. Astron. Soc. **25**, 1248 (1993).
[8] R. C. Hogan *et al.* (unpublished).
[9] A.B. Chhabra *et al.*, Phys. Rev. A **40**, 5284 (1989).
[10] C. Meneveau and K.R. Sreenivasan, J. Fluid Mech. **224**, 429 (1991).
[11] R.S. Rogallo and P. Moin, Annu. Rev. Fluid Mech. **16**, 99 (1984).
[12] R. S. Rogallo, NASA Technical Report No. TM-81315 (1981).
[13] V. Eswaran and S.B. Pope, Comput. Fluids **16**, 257 (1988).
[14] M. Lee and W. C. Reynolds, Stanford University, Department of Mechanical Engineering Technical Report No. Rep TF-24 (1985).
[15] H. Tennekes and J. L. Lumley, *A First Course in Turbulence* (MIT Press, Cambridge, MA, 1972).
[16] C. Meneveau and K.R. Sreenivasan, Phys. Rev. Lett. **59**, 1424 (1987).
[17] U. Frisch, *Turbulence* (Cambridge University Press, Cambridge, U.K., 1995), Chap. 8.
[18] M. Nelkin, Phys. Rev. A **42**, 7226 (1990).
[19] W. van de Water and P. Schram, Phys. Rev. A **37**, 3118 (1988).
[20] A.B. Chhabra and R.V. Jensen, Phys. Rev. Lett. **62**, 1327 (1989).
[21] D. W. I. Rouson *et al.*, Stanford University Technical Report No. TSD-101 (1997).
[22] B.K. Shivamoggi, Physica A **221**, 460 (1995).
[23] I. Hosokawa and K. Yamamoto, Phys. Fluids A **2**, 889 (1990).
[24] M.R. Maxey, Phys. Fluids **30**, 1915 (1987).